ISSN 1392-1207. MECHANIKA. Vol. 30, No. 5, 2024: 449–457

Stress Analysis of Vibrating Screen Side Plate based on Elastic Theory

Zongpeng ZHANG*, Ning WANG, Kunpeng PI***, Zhanxian WU****, Ming SU*****, Dongmin ZHU******, Zhiping XIE*******, Quan WU********, Man PENG*********, Rong LI************

**School of Mechanical and Electrical Engineering, Guizhou Normal University, Huaxi University Town, Gui'an New District, Guizhou Province, China, E-mail: zhangzongpeng0421@qq.com*
***School of Mechanical and Electrical Engineering, Guizhou Normal University, Huaxi University Town, Gui'an New District, Guizhou Province, China, E-mail: wn1262495266@163.com*
****Fuai Electronics (Guizhou) Co., Ltd, Gui'an New District, Guizhou Province, China, E-mail: 1961444502@qq.com*
*****CINTEC HEAVY EQUIPMENT TECHNOLOGY CO., LTD, Guiyang, Guizhou, China, E-mail: wu.zhanxian@qq.com*
******CINTEC HEAVY EQUIPMENT TECHNOLOGY CO., LTD, Guiyang, Guizhou, China, E-mail: suming629@163.com*
*******CINTEC HEAVY EQUIPMENT TECHNOLOGY CO., LTD, Guiyang, Guizhou, China, 312261824@qq.com*
********School of Mechanical and Electrical Engineering, Guizhou Normal University, Huaxi University Town, Gui'an New District, Guizhou Province, China, E-mail: xzpfeiniao@163.com*
*********School of Mechanical and Electrical Engineering, Guizhou Normal University, Huaxi University Town, Gui'an New District, Guizhou Province, China, E-mail: 23984943@qq.com*
**********School of Big Date and Computer Science, Guizhou Normal University, Huaxi University Town, Gui'an New District, Guizhou Province, China, E-mail: pengman1001@163.com*
***********School of Mechanical and Electrical Engineering, Guizhou Normal University, Huaxi University Town, Gui'an New District, Guizhou Province, China, E-mail: 460124215@gznu.edu.cn (Corresponding author)*

https://doi.org/10.5755/j02.mech.37285

1. Introduction

A vibrating screen serves as ubiquitous screening equipment in engineering. Its side plates and beams constitute critical and delicate components. Stress analysis and modeling of this type of part can be proved to be effective in suppressing the occurrence of damage, and the service life of the equipment can be effectively extended. Presently, there are several prevalent stress analysis methods, namely, analytical, numerical, and experimental methods. In practical applications, researchers meticulously choose one or a combination of these methods, depending on the specific research objectives, to ensure precision and accuracy in their findings. Mancini F. et al. [1] employed the nonlinear finite element analysis method to assess the deformation amplitude of thin-walled panels subjected to uniaxial tension. Their findings highlighted the significant role of early simplified structural stress assessments in bridging the divide between intricate numerical analyses and straightforward analytical schemes. Meriem Belhaou et al. [2] utilized both analytical and numerical methods to investigate the residual stress distribution within the nonlinear compression behavior of thick-walled cylinders composed of functionally graded materials. In the study of vibrating screens, various numerical techniques, including finite element analysis and modal analysis, are employed to thoroughly investigate the stress experienced by these screens. This comprehensive analysis offers robust support for enhancing the structural optimization of vibrating screens. Guo Nianqin and his team [3] also utilized ANSYS to assess the dynamic characteristics of the ultra-heavy vibrating screen's screen box structure, subsequently improving its design based on stress analysis. Hou Yongjun and his team [4] conducted finite element analysis on a dual-frequency vibrating screen box, examining its stresses, strengths, and lifespan to identify regions with reduced fatigue strength. Li Yumei et al. [5] employed ANSYS for modal analysis of the vibrating screen box, focusing on enhancing its reliability index to address challenges encountered in practical applications. Khoshdast, H. et al. [6] conducted a study on the dynamic stresses in vibrating screens utilized in the aggregate industry, employing the finite element method. The findings revealed that the employment of vibration dampers effectively mitigates the intense vibration energy within the screen mesh, thereby preventing any potential damage. While the numerical method has indeed been utilized in predicting potential failures and optimizing the design of vibrating screens, it is susceptible to various factors that can lead to its malfunction during usage. This malfunction can not only compromise production efficiency but also pose potential safety risks. Fang Peng [7] and his colleagues addressed the issue of failure in specific working conditions by optimizing the banana-type vibrating screen's performance, enhancing its overall functionality to meet operational requirements and resolve issues of malfunction. Wu Zhanxian et al. [8] integrated the optimization of the screen body structure with practical working conditions, conducting structural response analysis and stress analysis of the screen box to ensure its compliance with standards and mitigate the issue of side plate cracking. S. R. Allah Karam et al. [9] utilized scanning electron microscopy to analyze the ports of a vibrating screen's side plates, discovering that the bolted joints connecting the side plates to the screen frames were susceptible to crack propagation due to cyclic stresses, ultimately leading to failure.

Although the aforementioned methods facilitate the numerical investigation of stress distribution and fail-

ure reasons in vibrating screen designs, they fail to offer clarity on the genesis of local stress and its distribution patterns. To gain a deeper understanding of the local stress distribution and its evolution during the stable operation of the vibrating screen box, the theoretical modeling is built, the stress distribution is simulated, and various structures is compared. In the end, the practical performances are tested under different structures by vibration testing equipment. It offers a novel methodology for studying the stress distribution within the vibrating screen box side plate.

2. Mathematical Modeling

2.1. Principles of operation and theoretical assumptions

The three-axis elliptical horizontal vibrating screen analyzed in this paper is powered by a three-phase asynchronous motor. The gear system efficiently transmits power to rotate the excitation shafts of the eccentric rotor. The phase difference and installation angle between the excitation shafts of the eccentric rotor are precisely controlled and interconnected through transmission gears with identical modules and tooth counts, enabling the eccentric rotor to generate the desired excitation force and direction. The intricate structure of mechanism is depicted in Fig. 1.

As shown in Fig. 1, this kind of vibrating screen realizes the synchronous movement of three axes through three meshing gears, in which the movement direction of axis 1 and 3 is opposite to that of axis 2. There is an eccentric rotor fixed at the end of the shaft, which is driven by a motor to realize a certain frequency of vibration. The screen body studied in this paper will be subjected to alternating stresses in addition to material forces during the rotation of the eccentric rotor. Therefore, the study of the local stress distribution of the vibrating screen side plate can provide a new method for the study of the stress distribution inside the side plate of the vibrating screen box.

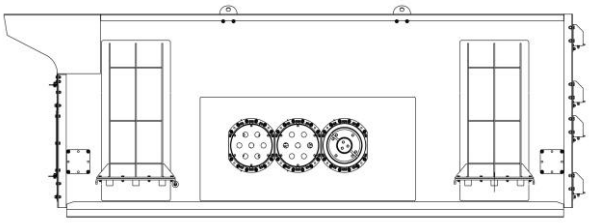

a

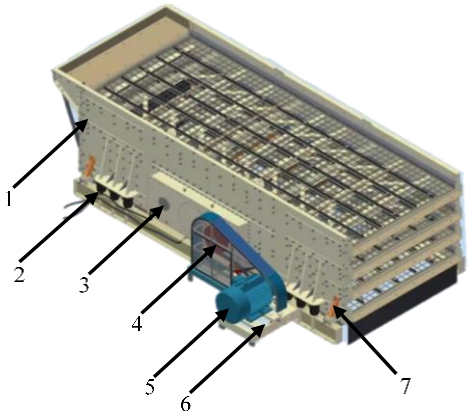

b

Fig. 1 Three-axis elliptical horizontal vibrating screen: a – vibrating screen side plate gear end; b – side view structure: *1* – side plate, *2* – rubber spring, *3* – vibration exciter, *4* – transmission device, *5* – motor, *6* – chassis, *7* – damper

Due to the significant excitation force, the presence of an eccentric rotor causes uneven stress distribution within the side plate and support beam, leading to a high risk of stress concentration. Given that the vibrating screen box is constructed from structural steel, it exhibits linear elastic behavior within its yield strength, yet there is a considerable size disparity between the side plate and support beam. As depicted in Fig. 1, the vibrating screen box features thin-walled symmetrical structures on both sides. To simplify the calculation of plane stress, the three-dimensional side plate and the support beam are assumed to be two-dimensional thin plates, which is beneficial to accurately evaluate the stress distribution in the sieve box.

2.2. Plane stress modeling of side plate

During the stable operation of a vibrating screen, it exhibits three degrees of freedom. When analyzing the side plate, given that rotation does not impact the plane of the side plate, it can be inferred that there are solely two stresses acting in the x and y directions within the side plate. Specifically, the force exerted near the holes in the side plate comprises a total of three round holes, as depicted in Fig. 2. Since the material of the screen box belongs to a linear elastic body, the superposition principle applies, thus enabling the analysis of a single round hole as a representative case.

Hence, let the radius of the circular hole be designated as '*a*', and introduce a concentric circle having a radius of '*b*'. On this outer circle, the impact of the circular hole on the stress distribution within the thin plate can be disregarded. Referring to the Fig. 2 at this juncture, a triangular element on a circle with radius ' $r = b$ ' is considered. Denote the length of the oblique side of this micro-element as 'd_s', and the stress components as σ_r and $\tau_{r\theta}$, as depicted

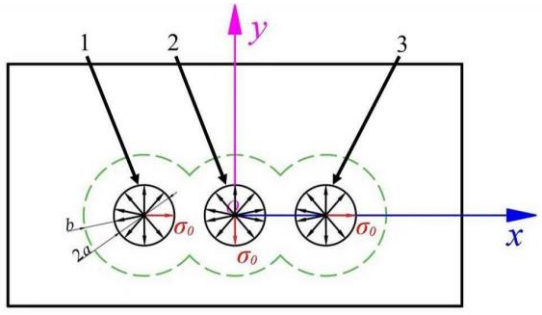

Fig. 2 Plane stress model of side plate

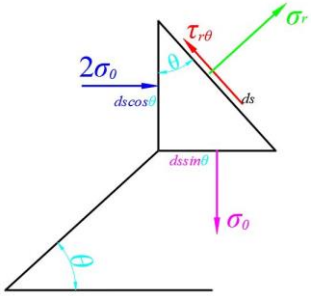

Fig. 3 Solid unit model

in Fig. 3. During the system was running, the direction of the excitation force generated by the 1-hole and the 3-hole was same, and the phase of the excitation force in the 2-hole would be lagged 90° than 1-hole and the 3-hole. The internal pressure value of each hole was also the same when the system was running under certain moment, so according to the principle of stress superposition, it can be considered that the horizontal stress was twice the vertical stress.

The equation of force equilibrium for a micro-unit is shown Eq. (1) and Eq. (2).

$$\sum F_r = 0: \ \sigma_r d_s + 2\left(\sigma_0 d_s \cos\theta\right)\cos\theta - \left(\sigma_0 d_s \sin\theta\right)\sin\theta = 0, \tag{1}$$

$$\sum F_\theta = 0: \ \tau_{r\theta} d_s - 2\left(\sigma_0 d_s \cos\theta\right)\sin\theta - \left(\sigma_0 d_s \sin\theta\right)\cos\theta = 0. \tag{2}$$

Solve the equation to determine its solution.

$$\begin{cases} \sigma_r = -\dfrac{1}{2}\sigma_0 - \dfrac{3}{2}\sigma_0 \cos 2\theta, \\ \tau_{r\theta} = \dfrac{3}{2}\sigma_0 \sin 2\theta. \end{cases} \tag{3}$$

The stress in Eq. (3) is treated as an external load and divided into two different sets of loads. The expression of the first set of loads is as Eq. (4).

$$\begin{cases} (\sigma_r)_b = -\dfrac{1}{2}\sigma_0, \\ (\tau_{r\theta})_b = 0. \end{cases} \tag{4}$$

Under the influence of this set of loads, the force distribution is analogous to the condition where the annular plate is uniformly exposed to internal pressure, resulting in a compressive stress distribution as depicted in Fig. 4.

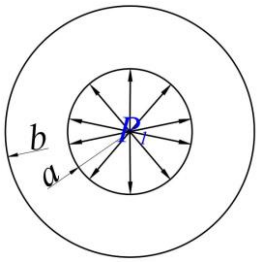

Fig. 4 Force under the initial loading

By utilizing the thick-walled cylinder formula [10] and incorporating $P_1=0.5\sigma_0$, $P_2=0$ into calculations, Eq. (5) can be obtained.

$$\begin{cases} \sigma_r = \dfrac{a^2}{b^2-a^2}\dfrac{\sigma_0}{2}\left(1-\dfrac{b^2}{r^2}\right), \\ \sigma_\theta = \dfrac{a^2}{b^2-a^2}\dfrac{\sigma_0}{2}\left(1+\dfrac{b^2}{r^2}\right), \\ \tau_{r\theta} = 0. \end{cases} \tag{5}$$

The formula representing the second set of loads is given by:

$$\begin{cases} (\sigma_r)_b = -\dfrac{3}{2}\sigma_0 \cos 2\theta, \\ (\tau_{r\theta})_b = \dfrac{3}{2}\sigma_0 \sin 2\theta. \end{cases} \tag{6}$$

Due to the existence of various factors within this set of loads, such as $\cos 2\theta$, $\sin 2\theta$. Drawing from the established relationship between stress and the stress function [10], the Eq. (7) can be deduced.

$$\begin{cases} \sigma_{\mathrm{r}} = \dfrac{1}{r}\dfrac{\partial\varphi}{\partial r} + \dfrac{1}{r^2}\dfrac{\partial^2\varphi}{\partial\theta^2}, \\ \sigma_\theta = \dfrac{\partial^2\varphi}{\partial r^2}, \\ \tau_{\mathrm{r}\theta} = -\dfrac{\partial}{\partial r}\left(\dfrac{1}{r}\dfrac{\partial\varphi}{\partial\theta}\right). \end{cases} \tag{7}$$

Assuming the stress function is defined as follows: $\varphi = f(r)\cos 2\theta$. By substituting the deformation coordination formula [10] the Eq. (8) result can be obtained.

$$\left(\frac{\partial^2}{\partial r^2} + \frac{1}{r}\frac{\partial}{\partial r} + \frac{1}{r^2}\frac{\partial^2}{\partial\theta^2}\right)\left(\frac{\partial^2\varphi}{\partial r^2} + \frac{1}{r}\frac{\partial\varphi}{\partial r} + \frac{1}{r^2}\frac{\partial^2\varphi}{\partial\theta^2}\right) = 0. \tag{8}$$

Solve the equation to determine its solution shown in Eq. (9):

$$\left(\frac{d^2}{dr^2} + \frac{1}{r}\frac{d}{dr} - \frac{4}{r^2}\right)\left(\frac{d^2 f}{dr^2} + \frac{1}{r}\frac{df}{dr} - \frac{4f}{r^2}\right) = 0. \tag{9}$$

The general solution of this equation is as follows: $f(r)=Ar^2+Br^4+C/r^2+D$. So, $\varphi=(Ar^2+Br^4+C/r^2+D)\cos 2\theta$. Furthermore, the expression of the stress component can be derived as Eq. (10):

$$\begin{cases} \sigma_r = -\left(2A + \dfrac{6C}{r^4} + \dfrac{4D}{r^2}\right)\cos 2\theta, \\ \sigma_\theta = \left(2A + 12Br^2 + \dfrac{6C}{r^4}\right)\cos 2\theta, \\ \tau_{r\theta} = \left(2A + 6Br^2 - \dfrac{6C}{r^4} - \dfrac{2D}{r^2}\right)\cos 2\theta. \end{cases} \tag{10}$$

The second set of load boundary conditions comprises as Eq. (11):

$$\begin{cases} r=b:\sigma_r=-\dfrac{3}{2}\sigma_0\cos 2\theta,\ \tau_{r\theta}=\dfrac{3}{2}\sigma_0\sin 2\theta, \\ r=a:\sigma_r=\sigma_0,\ \tau_{r\theta}=0. \end{cases} \tag{11}$$

Where $r = a$, the stress is uniformly distributed across the interior surface of the circular hole.

The four equations are derived as follows:

$$\begin{cases} 2A+\dfrac{6C}{b^4}+\dfrac{4D}{b^2}=\dfrac{3}{2}\sigma_0, \\ 2A+6Bb^2-\dfrac{6C}{b^4}-\dfrac{2D}{b^2}=\dfrac{3}{2}\sigma_0, \\ 2A+\dfrac{6C}{a^4}+\dfrac{4D}{a^2}=\sigma_0, \\ 2A+6Ba^2-\dfrac{6C}{a^4}-\dfrac{2D}{a^2}=0. \end{cases} \tag{12}$$

Since b must be sufficiently large and $(b/a) \approx 0$, the results can be solved: $A = 0.75\sigma_0$, $B = 0$, $C = -0.75\sigma_0$, $D = a^2\sigma_0$.

Substituting the solution data into the stress component equation and the results can be got like as Eq. (13):

$$\begin{cases} \sigma_r=-\dfrac{1}{2}\sigma_0-\left(\dfrac{3}{2}\sigma_0-\dfrac{9a^4}{2r^4}\sigma_0+\dfrac{4a^4}{r^2}\sigma_0\right)\cos 2\theta, \\ \sigma_\theta=\dfrac{1}{2}\sigma_0+\left(\dfrac{3}{2}\sigma_0-\dfrac{9a^4}{2r^4}\sigma_0\right)\cos 2\theta, \\ \tau_{r\theta}=\left(\dfrac{3}{2}\sigma_0+\dfrac{9a^4}{2r^4}\sigma_0-\dfrac{2a^4}{r^2}\sigma_0\right)\sin 2\theta. \end{cases} \tag{13}$$

During the running of the vibrating screen, σ_0 represents the initial stress.

Upon examining the stress component formula of the side plate, the trend of the plane stress of the eccentric rotor in the side plate is obviously seen to show an obvious periodic mode, with the stress in each direction being intricately linked to the initial stress.

3. Simulation Results and Analysis

After conducting theoretical calculations and modeling, a preliminary understanding of the plane stress distribution within the side plate has been achieved. Typically, the existing screen body structure relies on a motor to generate excitation vibration through an eccentric block, causing the entire screen body to vibrate. Notably, the eccentric rotor applies force to only one side of the side plate. This configuration is illustrated in Fig. 5, a. However, this structure results in the excitation source creating a moment on the side plate, which is detrimental to the force distribution within the side plate. To address this issue, a symmetrical distribution of the excitation source structure is proposed, as depicted in Fig. 5, b. By modeling the stress component equation, the impact of each parameter on the individual stress components has been thoroughly analyzed.

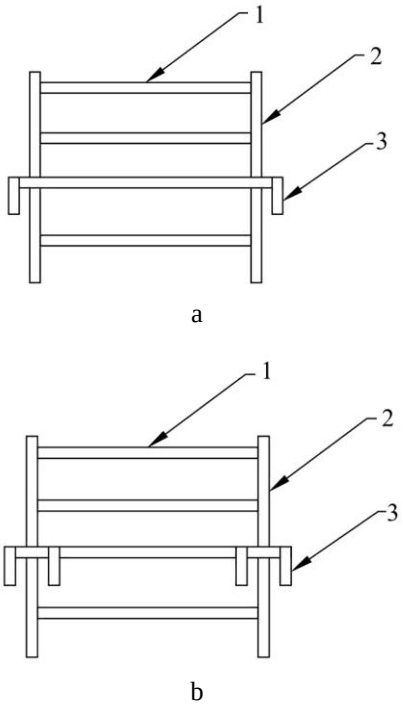

Fig. 5 Two methods of exciting source arrangement: a - distributed asymmetrically on one side of the side plate: *1* – screen holder, *2* – side pane1, *3* – eccentric rotor, b - symmetrically distributed on the side plates: *1* – screen holder, *2* – side pane1, *3* – eccentric rotor

3.1. Analysis and Discussion of Simulation

3.1.1. Unilateral asymmetric structure

The vibrating screen box is constructed from two side plates. Since the eccentric rotor exerts a unilateral force on the side plate, it is imperative to conduct a plane stress analysis of the side plate to comprehend the stress induced by the excitation force on the material. Given the presence of three holes in the side plate where the eccentric rotor is mounted, the excitation force exerted by the rotor can be deemed as an initial stress for the side plate. This initial stress serves as the basis for analyzing the radial, circumferential, and shear stresses surrounding the holes in the side plate.

Fig. 6 illustrates the distribution of radial stress values within the polar axis stress component equation surrounding the hole. It is evident from the figure that the stress value initially rises, peaks, and then gradually tapers off, stabilizing at a certain value as the distance from the hole increases. Due to the presence of the hole in the side plate, a peak stress emerges in the adjacent area, resulting in a maximum stress level that is 2.5 times higher than the initial stress. Notably, the direction of this peak stress opposes the initial stress direction. Since the initial stress is determined by the motor's performance and the eccentric rotor's interaction with the side plate, the side plate's stress expression is typically compressive. Therefore, the peak stress observed in the side plate represents its maximum tensile stress. In the area where the maximum tensile stress occurs, a periodic stress cycle occurs, and the possibility of forming cracks at the threaded connection of the side plate is significantly increased.

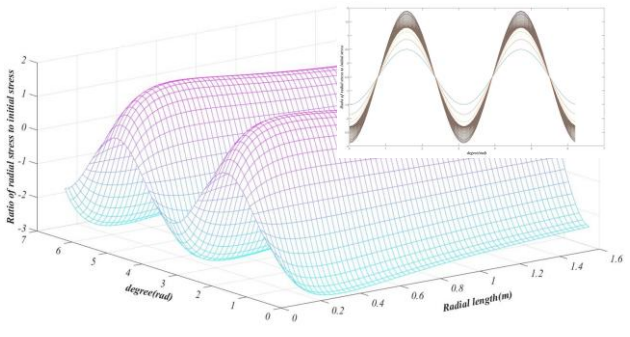

Fig. 6 Radial stress distribution diagram

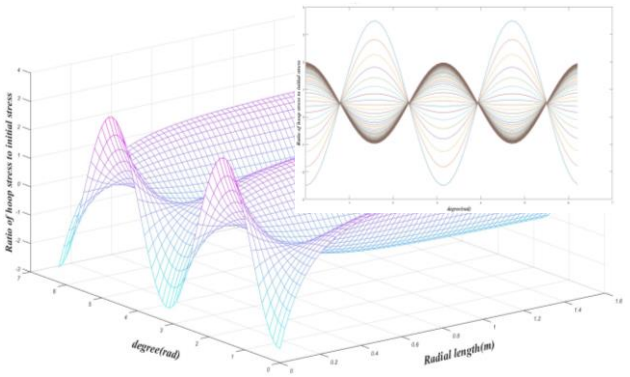

Fig. 7 Circumferential stress distribution

Fig. 7 illustrates the hoop stress distribution in the plane stress component equation proximal to the hole. Evidently, the stress value exhibits an initial decrease followed by an increase with increasing distance from the hole, ultimately stabilizing. In the polar angle direction of the element, tensile and compressive stresses alternate. During the two periods of eccentric rotor excitation, the hoop stress of the side plate exhibits a triangular function distribution, aligning with the actual excitation force direction of the vibrating screen. Additionally, due to the circular hole in the side plate, the hoop stress experiences a zero-value state, resulting in concurrent tensile and compressive stresses. Consequently, the presence of a tip in the threaded hole on the side plate can induce expansion through the tip, leading to high stress concentrations that yield the material in a localized region and ultimately leading to fracture.

Fig. 8 illustrates the distribution of shear stress values within the plane stress component equation surrounding the side plate hole. The graph reveals a decrease in stress values as the distance from the hole increases, until a certain point where the shear stress stabilizes at a constant value. Furthermore, the shear stress exhibits a trigonometric function distribution. The graphical representation of shear stress demonstrates that as the distance from the initial force position decreases, the shear stress increases. Additionally, during the excitation of the unidirectional eccentric rotor, shear stress acts perpendicular to the side plate, peaking at 3-4 times the initial stress level.

3.1.2. Bilaterally symmetric structure

When the eccentric rotor of the vibrating screen is positioned on both sides of the side plate, the excitation force imparted to the entire system remains unchanged compared to when it was situated solely on one side. Consequently, in accordance with the superposition principle and Saint-Venart principle in elastic theory, the plane

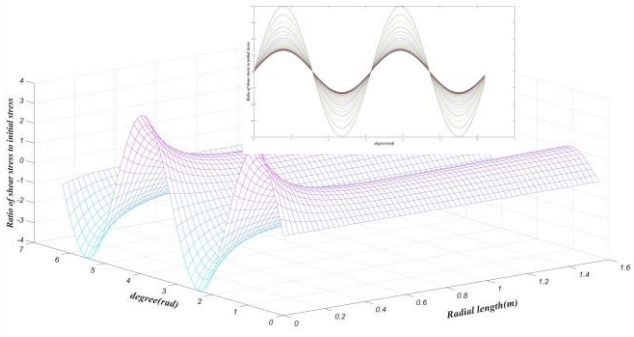

Fig. 8 Shear stress distribution

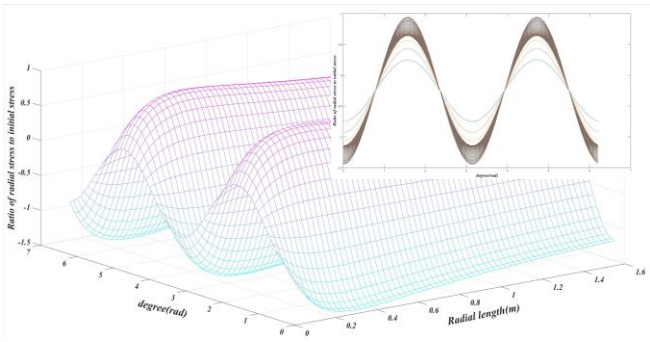

Fig. 9 Radial stress distribution

stress distribution within the symmetrical structure on both sides can be considered equivalent to half of that observed in the asymmetrical structure on one side. Therefore, for symmetrical structures, the author only selects one side of the side plate for analysis.

Fig. 9 depicts the radial distribution of stress component values surrounding a hole in a symmetrical structure. Upon observing the figure, it becomes evident that the stress values initially increase, reaching a peak before gradually decreasing and stabilizing as the distance from the hole increases. Notably, the ratio of stress values to the initial stress on one side of the side plate oscillates close to 1, while the peak stress multiplier reaches nearly 1.5 times the original value, but in the opposite direction. Since the initial force direction corresponds to compressive stress, the stress on the opposite side of the hole exhibits a superimposed state, resulting in two distinct types of stress: tensile and compressive, varying in magnitude. Since the initial stress arises from the motor's interaction with the eccentric rotor against the side plate of the vibrating screen, the side plate should primarily experience compressive stress. Therefore, the maximum tensile stress in the side plate is represented by the peak stress on the other side of the device. Although the symmetrical design distributes the maximum tensile stress evenly across both sides of the side plate, reducing the risk of periodic stress fatigue, it also mitigates the peak value of the maximum tensile stress.

The hoop stress distribution diagram depicted in Fig. 10 illustrates the distribution of stresses around a hole in the side plate of a symmetrical structure, calculated using the plane stress component formula in the polar angle direction. The diagram reveals that the stress value decreases initially, followed by an increase as the distance from the hole increases, ultimately reaching a stable trend.

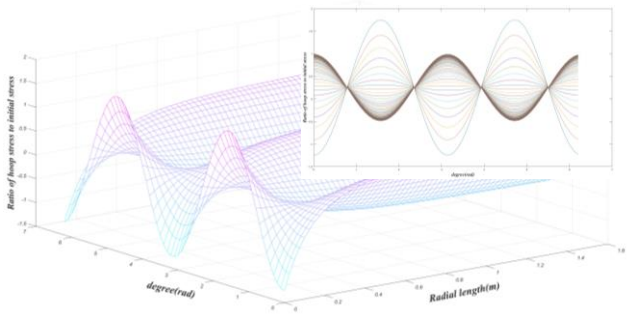

Fig. 10 Circular stress distribution

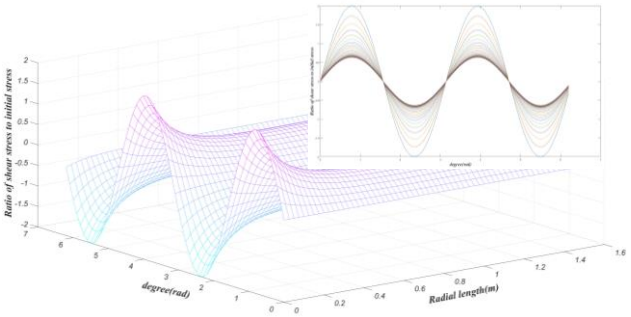

Fig. 11 Single shear stress distribution

Additionally, in the polar axis direction of polar coordinates, the plane stress of the side plate experiences a reciprocal transformation between tensile and compressive stresses. Over the course of two cycles of eccentric rotor rotation, the hoop stress distribution of the side plate exhibits a triangular function, with the direction of hoop stress distribution aligning with the actual exciting force of the vibrating screen. A zero point is identified in the hoop stress distribution diagram of the side plate, resulting in the concurrent existence of hoop tension and compression stress.

Fig. 11 illustrates the distribution of shear stress values within the plane stress component encircling the hole in the side plate of a symmetrical structure. It is evident from the diagram that the stress values gradually diminish as the distance from the hole increases; however, after a certain distance, the shear stress stabilizes to a constant value. Additionally, the shear stress exhibits a trigonometric function distribution pattern. It can be observed that the shear stress intensifies as the distance from the initial stress decreases in the side plate in a symmetrical structure. During the excitation of a bi-directional eccentric rotor, the shear stress is oriented towards the side plate, resulting in a maximum shear stress peak value that is reduced by half compared to that of a single direction, thereby enhancing the service life of the side plate to a certain extent.

3.1.3. Discussion of comparison results

The schematic diagram of plane stress for a bilaterally symmetrical structure is depicted in Fig. 12. The theoretical calculations for the vibrating screen are founded on unidirectional asymmetric excitation force, analogous to stress analysis within a unidirectional two-dimensional plane of the side plate. Consequently, the initial stress on one side diminishes in comparison to the other, manifesting a deformation trend from the exterior towards the interior of the side plate. Additionally, the stress component calculated based on plane stress theory incorporates an inward shear stress, elevating the likelihood of side plate deformation. Notably, the plane stress on one side of the side plate in the symmetrical structure depicted in Figs. 9, 10 and 11 is half that of the unidirectional asymmetric structure. Furthermore, as the eccentric rotors on both sides exhibit identical movement trends relative to the side plate, the plane stress distribution across both sides remains symmetrical with respect to the side plate. Consequently, it can be inferred that the radial and hoop stresses of the side plate in the symmetrical structure align in the same direction. The shear stress on both sides causes the outer shear stress to direct inward due to the symmetrical structure relative to the side plate. Conversely, the shear stresses inside are outward and equivalent in magnitude, effectively cancelling each other out on the inside and outside of the side plates. In real device, the ductile cracks is shown in the side plates of the asymmetrical structure, as shown in Fig. 13. It is due to the asymmetrical structure leading to the formation of periodic cyclic stresses, which in turn lead to plate stress fatigue.

Therefore, despite the fact that the symmetrical structure of the eccentric rotor distribution does not alter the periodic stress situation, it effectively minimizes the peak value of plane stress, diminishes the chances of stress concentration, and mitigates the likelihood of material yield phenomena. To enhance the durability and lifespan of the side plate, thin plates made of identical material are integrated between the side plate, gear end, and motor end, bolstering the side plate's strength. The initial stress of the system is excited by the eccentric rotor driven by the motor, which is caused by the impact of the drive shaft on the side plate. The middle reinforcing plate serves to mitigate the impact during startup and shutdown and the periodic stress on the side plate during steady-state operation, ultimately extending the side plate's service life.

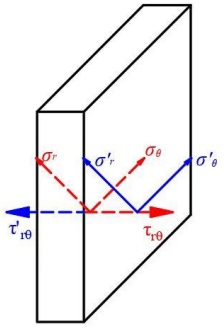

Fig. 12 Plane stress diagram of symmetrical position on both sides of side plate

Fig. 13 Ductile cracks of side plan

4. Test Results and Analysis

4.1. Test preparation

Fig. 14 shows the rotor end of the vibrating screen, which is arranged on the outside of the two side plates of the vibrating screen with the gear end of Fig. 1. In the experiment, both the rotor end and the gear end will be wrapped by the housing, and for better measurement of the stress in the holes, the strain gauges are pasted on the inside of the side plates near the small holes.

Fig. 14 Vibrating screen rotor end: *1* – transmission shaft, *2* – eccentric rotor

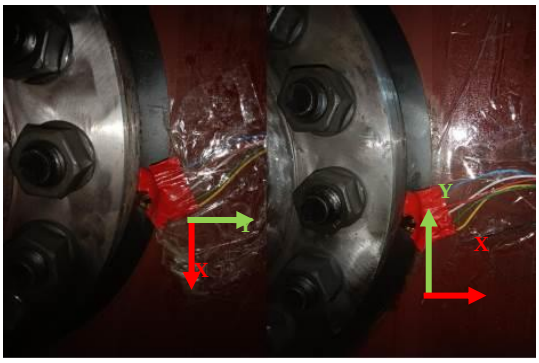

a

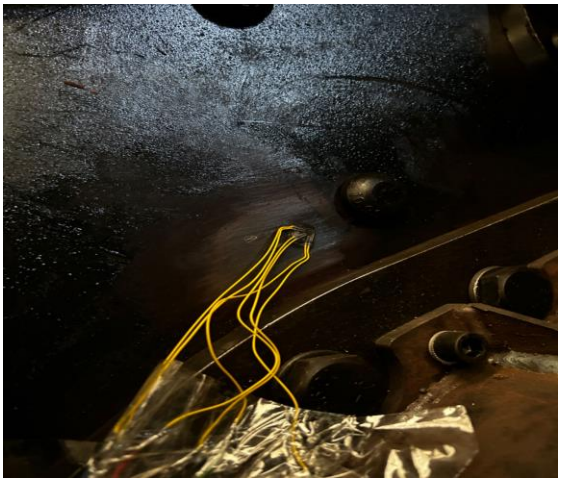

b

Fig. 15 Actual test position: a – gear-end strain gauges affixed horizontally and vertically, b – rotor end strain gauge paste diagram

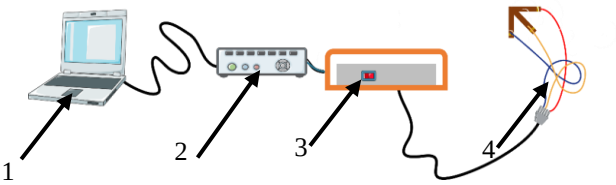

Fig. 16 Test instrument and connection method: *1* – Vibration analysis software, *2* – Vibration signal acquisition instrument, *3* – Strain conditioner, *4* – Strain gauge

Prior to measuring the stress on the sieve box part, it is imperative to establish the optimal position for stress measurement. As shown in Fig. 15, a and b, the measured position can be measured and is closest to the center of the hole. The Y direction pointing towards the drive shaft in the diagram represents the radial direction in Fig. 15, a, and X is the surface of the circular hole represents the circumferential direction. Subsequently, the strain gauge must be securely welded, with the cable soldered to the strain conditioner, to ensure consistent and reliable data input throughout the testing phase. Furthermore, specialized cables must be used to establish a secure connection between the vibration signal acquisition instrument and the strain conditioner. It is essential to maintain a strict one-to-one correspondence during the connection process to prevent any confusion in measurement outcomes. The test equipment used in the experiment was INV3062S dynamic acquisition instrument and INV1861 strain conditioner manufactured by Beijing Oriental Institute of Vibration and Noise Technology.

4.2. Test results

Based on the aforementioned modeling and analysis of the side plate of the vibrating screen box, a field test is conducted on the screen box structure, comparing the asymmetric structure of a unilateral rotor with the symmetric structure of a bilateral rotor relative to the side plate. This comparison is achieved using stress testing equipment, and the stress levels on the side plate are evaluated through the collected data.

Fig. 17 reveals that the plane stress around the side plate hole exhibits periodicity, regardless of whether the rotor arrangement is unilateral or bilaterally symmetrical. In the unilateral distribution system, the actual measurement of the motor and gear at the same end of the vibrating screen, while in the bilateral distribution system, the position of the motor and gear are located at both ends of the vibrating screen. In addition, the strain flower measurement position is affected by the actual situation (including oil contamination, reinforcing plate, etc.), the measurement of the side plate stress at the motor and gear end is selected as a position on the side plate closest to the center of the hole. Notably, the stress values of the bilateral arrangement are approximately half of those observed in the unilateral configuration, both at the maximum and minimum principal stress levels. However, exceptionally high stress values are observed at motor end 2 and gear end 2 of the double-sided rotor. This elevated stress may be attributed to oil leakage within the side plate plane, potentially leading to insufficient adhesion of the strain gauge. Once the vibrating screen is activated, the strain gauge

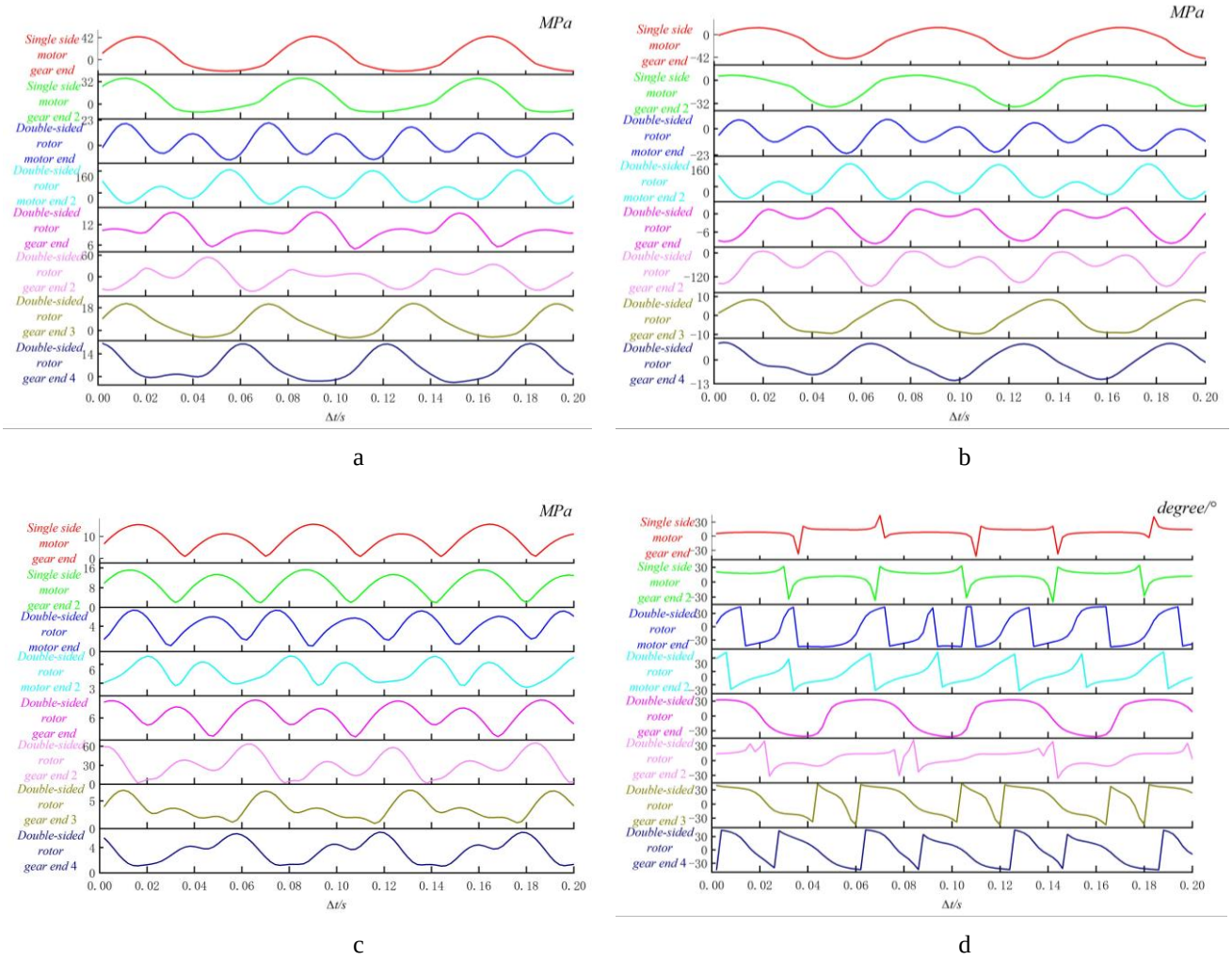

Fig. 17 Stress test results near side plate holes in two structures: a – maximum principal stress distribution, b – minimum principal stress distribution, c – maximum shear stress distribution, d – angle distribution of principal stress and 0°

enters a state of near-unload, resulting in a discrepancy with theoretical predictions. During actual measurements, both strain gauges at this position detached, prompting subsequent tests on gear ends 3 and 4 to corroborate our hypothesis. Consequently, these two datasets are unsuitable for comparative analysis based on the available measurement conditions. Excluding these datasets, the in-plane stresses for the remaining four double-sided rotor configurations are approximately half that of the single-sided rotor, following the same trend derived from a comparison of the two-dimensional plots in Figs. 6 and 9, 7 and 10 showing where the stresses are concentrated.

5. Conclusions

By modeling the plane stress within the side plates of the triaxial oval horizontal screen's screen box structure, we conducted on-site stress testing and compared it with the model derived from mathematical modeling. There are two conclusions is received as following.

1. The mathematical model developed to represent the combined stresses in the plane of the vibrating screen side plates shows the same trend as the actual combined stress distribution measurements and both are periodic. The stress distribution in the side plate is accurately described by the model, especially when considering the unilateral and bilateral distributed excitation rotors.

2. With a symmetrically distributed structure, the peak stress of the side plate is reduced to half that of a single-sided structure, while the superposition of shear stress on both sides effectively mitigates the shear stress on the side plate.

Acknowledgement

This research was financially supported by the Guizhou Industry Simulation Design & Innovation Center (QKZYD NO. [2016]4006). Moreover, this research was also financially supported by Guizhou Education Department Science and Technology Research Project Serve for the "Four New" and "Four Modernization" (QJJ [2022] No. 005) and the Aerospace and Equipment Manufacturing Industry Mentor Group Project (C424013/118).

References

1. **Mancini, F.; Remes, H.; Romanoff, J.** 2024. On the modelling of distorted thin-walled stiffened panels via a scale reduction approach for a simplified structural stress analysis, Thin-Walled Structures 197: 111637. https://doi.org/10.1016/J.TWS.2024.111637.
2. **Belhaou, M.; Laghzale, N. E.; Bouzid, A. H.** 2024. Residual stresses in autofrettaged functionally graded

pressurized thick cylinders, International Journal of Pressure Vessels and Piping 208: 105143. https://doi.org/10.1016/J.IJPVP.2024.105143.
3. **Nianqin, G.; Sheng, G.; Leping, L.** 2010. Modal Characteristics and Finite Element Analysis of Screen Box for Ultra-heavy Vibrating Screen, proceedings of the 2010 Third International Conference on Information and Computing, F, IEEE: 284-287. https://doi.org/10.1109/ICIC.2010.343.
4. **Hou, Y. J.; Fang P.; Zeng, L.** 2012. Finite element analysis of dual-frequency vibrating screen, proceedings of the Advanced Materials Research, F, Trans Tech Publ: 2124-2128. https://doi.org/10.4028/www.scientific.net/AMR.479-481.2124.
5. **Li, Y.; Jiang, L.** 2023. Reliability analysis of vibrating screen box based on finite element method, Paper Equipment and Materials 52(01): 11-13 (in Chinese).
6. **Khoshdast, H.; Khoshdast, H.; Jalilifard, S.** 2021. Dynamic analysis of a dashpots equipped vibrating screen using finite element method, Physicochemical Problems of Mineral Processing 57(1): 112-126. https://doi.org/10.37190/ppmp/130001.
7. **Fang, P.; Shen, Q.** 2023. Structural optimization design of banana type vibrating screen, Modern Industrial Economy and Informatization 13(01): 95-97+100. https://doi.org/10.16525/j.cnki.14-1362/n.2023.01.035.
8. **Wu, Z.; Liu, J.; Ran L.** et al. 2020. Dynamic stress analysis and structural optimization of horizontal screen body based on ANSYS Workbench, Equipment Manufacturing Technology (09): 43-47 (in Chinese).
9. **Karam, S. R. A.; Khodadad, M.; Talab, M. S.; Moeini, A.** 2009. FAILURE STUDY IN SIDE PLATES OF A VIBRATING SIEVE, International Journal of Mechanical and Materials Engineering 4(2): 118-122.
10. **Wang, Z.; Yuan, S.; Hu, L.** 2007. The fundamentals of Elastic and Plastic Mechanics. Harbin Institute of Technology Press (2nd Edition, in Chinese).

Z. Zhang, N. Wang, K. Pi, Z. Wu, M. Su, D. Zhu, Z. Xie, Q. Wu, M. Peng, R. Li

STRESS ANALYSIS OF VIBRATING SCREEN SIDE PLATE BASED ON ELASTIC THEORY

S u m m a r y

To accurately grasp the stress distribution within the side plate of the vibrating screen box, a mechanical model has been developed, grounded in the plane stress theory of elastic mechanics. This model has subsequently been utilized to predict the stress distribution within the side plate, particularly when subjected to excitation forces arising from both unilateral and bilateral rotor arrangement structures. The results reveal that the mechanical model, which is firmly based on elastic mechanics, effectively captures the intricate stress patterns within the perforated side plate structure. Notably, the peak stress in a symmetrically distributed structure is significantly reduced, being merely half of that observed in a unilateral configuration. Additionally, the shear stress accumulated on both sides of the side plate acts to balance and consequently reduce the overall shear stress experienced by the plate.

Keywords: theory of elasticity, plane stress distribution, structure optimization, vibration testing.

Received May 14, 2024
Accepted October 22, 2024